JACS
JOURNAL OF THE AMERICAN CHEMICAL SOCIETY
Communication
pubs.acs.org/JACS

Screening for Superoxide Reactivity in Li-O_2 Batteries: Effect on Li_2O_2/LiOH Crystallization

Robert Black,[‡] Si Hyoung Oh,[‡] Jin-Hyon Lee, Taeeun Yim, Brian Adams, and Linda F. Nazar*

Department of Chemistry, University of Waterloo, 200 University Avenue West, Waterloo, Ontario N2L 3G1, Canada

Supporting Information

ABSTRACT: Unraveling the fundamentals of Li-O_2 battery chemistry is crucial to develop practical cells with energy densities that could approach their high theoretical values. We report here a straightforward chemical approach that probes the outcome of the superoxide O_2^-, thought to initiate the electrochemical processes in the cell. We show that this serves as a good measure of electrolyte and binder stability. Superoxide readily dehydrofluorinates polyvinylidene to give byproducts that react with catalysts to produce LiOH. The Li_2O_2 product morphology is a function of these factors and can affect Li-O_2 cell performance. This methodology is widely applicable as a probe of other potential cell components.

The rechargeable nonaqueous lithium−oxygen cell is a promising large-scale energy storage system because of its high theoretical energy density (>3500 Wh/kg) and the possibility of using oxygen from air as a "fuel".[1] O_2 molecules are reduced on the positive electrode (oxygen reduction reaction, ORR) during discharge to produce an insoluble product, lithium peroxide (Li_2O_2), that deposits on or within the electrode pores. Recharging the cell oxidizes the Li_2O_2 to release O_2 and Li^+/e^- (oxygen evolution reaction, OER).[2] The overpotentials are high, ~0.3 V for ORR and >1.0 V for OER at a moderate current density, and catalysts are thought necessary to lower the activation energy at high discharge capacities. Many catalysts for ORR and OER adopted from aqueous metal−air and fuel cells have been investigated, such as α-MnO_2.[3−5] For Li-O_2 cells, discharge continues as long as active surface sites for ORR and pores for Li_2O_2 deposition are available.[6] A porous electrode is critical to achieve a high discharge capacity and efficient cycling.

The first step of ORR in nonaqueous electrolyte systems is considered to be the formation of lithium superoxide radicals.[7] Ideally, LiO_2 further reacts to form Li_2O_2 by either disproportionation ($2LiO_2 \rightarrow Li_2O_2 + O_2$) or electrochemical ($LiO_2 + Li^+ + e^- \rightarrow Li_2O_2$) routes.[8] However, the discharge product is not Li_2O_2 in many conventional electrolyte systems,[9−13] owing to the high nucleophilicity of the O_2^- radical. Propylene carbonate (PC), for example, is subject to ring-opening attack that produces a variety of organic lithium salts.[14] Salts such as lithium bis(oxalato)borate are decomposed to produce lithium oxalate.[15] Some ether-based electrolytes may also be reactive.[16] These reactions with superoxide radicals not only lead to depletion of the electrolyte but also alter the discharge product and thus fundamentally change the nature of the charge process. None of the conventional electrolytes are reported to be completely inert, although siloxane glycol derivatives may be particularly robust.[17] Thus, an easy first-step probe of the interaction of O_2^- with a variety of cell materials is critical to screen for the possibility of degradation. Side products from these reactions can cause increased polarization and suppress oxygen evolution, as does electrolyte reactivity.

Scheme 1. Exploratory Reactions of Superoxide That Parallel Those in a Li-O_2 Cell: (A) KO_2 + $LiPF_6$/TEGDME; (B) KO_2 + $LiPF_6$/TEGDME + Carbon; (C) Electrochemical Cell (Carbon Catalyst); (D) KO_2 + $LiPF_6$/TEGDME/PVdF; (E) KO_2 + $LiPF_6$/TEGDME/PVdF/α-MnO_2 Catalyst [KO_2 = KO_2 (Crown Ether)]

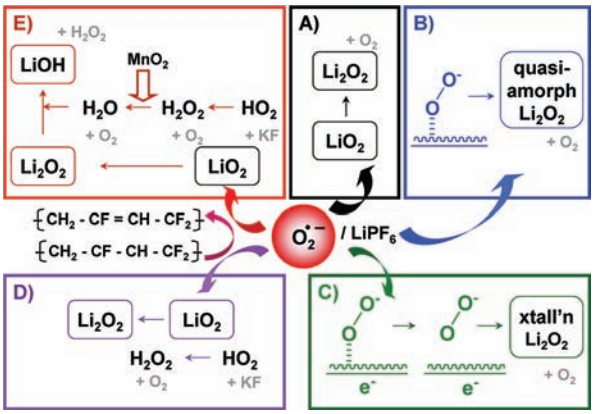

Here we report the reaction of chemically generated solvated superoxide radicals with materials typically used in a Li-O_2 cell—selected combinations of carbon black, poly(vinylidene difluoride) (PVdF) or Nafion binder, and catalyst (α-MnO_2)—and compare these to electrochemical Li-O_2 cells. We generated metastable superoxide from the well-known reaction of KO_2 with dicyclohexyl-18-crown-6 (crown ether) in solution, which complexes the K^+.[18] Metathesis with a lithium salt forms metastable solvated LiO_2 *in situ*. We show that the cell materials affect the outcome of the reactions that are the first steps in ORR in the Li-O_2 cell and determine the nature and morphology of the products (Li_2O_2/LiOH). This can affect electrochemical capacity and fading. The results summarized in Scheme 1 reveal that surprising sequences are responsible for some side reactions. Although PVdF and PC are both reactive,

Received: November 28, 2011
Published: January 27, 2012

   dx.doi.org/10.1021/ja2111543 | *J. Am. Chem. Soc.* 2012, 134, 2902−2905

surprisingly, tetraethylene glycol dimethyl ether (TEGDME) is relatively stable to superoxide attack.

Scheme 1A shows the effect of adding O_2^- to 1 M $LiPF_6$/TEGDME solution in the absence of any other components. Reaction of O_2^- with Li^+ was accompanied by evolution of O_2 gas and gradual precipitation of an off-white powder, shown to be crystalline Li_2O_2 by XRD (Figure 1a-i). This is formed by

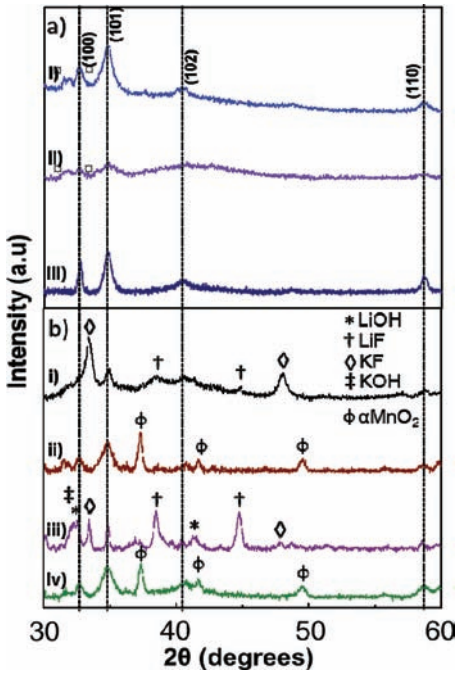

Figure 1. (a) Diffraction patterns for Li_2O_2 production using (i) $LiPF_6/KO_2$/TEGDME, (ii) $LiPF_6/KO_2$/TEGDME/carbon, and (iii) electrochemically discharged carbon cathode. (b) Diffraction pattern of washed products for the chemical reactions in Scheme 1A with added cathode components of (i) PVdF only, (ii) α-MnO_2 only, (iii) PVdF + α-MnO_2, and (iv) α-MnO_2 + Li-Nafion. Dashed vertical black lines on all patterns indicate Li_2O_2; ¤ = residual KO_2.

dismustase of the LiO_2 which initially forms in solution on salt metathesis, indicating that LiO_2 has some limited solubility in solution:

$$KO_{2(s)} + LiPF_{6(s)} \rightarrow LiO_2 + [K^+/\text{crown ether}]PF_6^-{}_{(s)} \quad (1)$$

$$2LiO_2 \rightarrow Li_2O_{2(s)} + O_{2(g)} \quad \text{(dismutation)} \quad (2)$$

The salt metathesis product, $[K^+/\text{crown ether}]PF_6$, was extracted from the solid, recrystallized as the salt, and unambiguously identified by XRD (Supporting Information (SI), Figure S1). To determine whether TEGDME suffered degradation/oxidative decomposition as a result of reaction with the free superoxide in the presence of O_2, we analyzed the solid product by ^1H and ^{13}C NMR. D_2O was added to dissolve any organic salts resulting from potential superoxide/O_2 attack on TEGDME[16] (i.e., lithium formate and/or lithium acetate) via conversion to their deuterated products, CH_3CO_2D and HCO_2D. The high concentrations afforded by the KO_2 reaction probe are expected to give clear evidence of these products should reactivity occur. Extraction of the solid product with D_2O showed no decomposed products in the ^1H NMR (see SI, Figure S2). The ^{13}C NMR spectrum of the solid extract also revealed *no* carbonyl peaks derived from acetate, formate, or other carboxylate decomposition products (SI, Figure S3). According to our spectroscopic results, TEGDME does not undergo significant reactivity like PC (see below). We do not discount the possibility of limited electrochemical reactivity of TEGDME, which might occur as a result of other cell byproducts such as HO_2/H_2O_2 (see below) or of repeated cycling in a cell that subjects the electrolyte to local overpotential on charge by reaction with Li_2O_2.

We explored the effect of adding O_2^- to a 1 M $LiPF_6$/PC solution to confirm the validity of the KO_2 reaction probe. This reaction results in extensive PC decomposition in Li-O_2 electrochemical cells.[14] In accord with those findings, addition of $LiPF_6$ to the KO_2[crown ether]/PC resulted in neither evolution of gas (O_2) nor precipitation of Li_2O_2. Instead, the ^1H NMR spectrum of the solid confirms all of the reported ring-opening products (SI, Figures S4 and S5) formed by attack of superoxide on PC,[14] which inhibit the formation of Li_2O_2. Thus, these reactions provide the basis of a good approach to explore the O_2^- reactivity toward the other components used in Li-O_2 cells.

In a Li-O_2 cell, the porous cathode is constructed from carbon black, which acts as an electronically conductive pathway for the ORR and OER reactions and houses the accumulation of Li_2O_2.[5] The effects of *chemically* generating LiO_2 in the presence of carbon in our reaction sequence are depicted in Scheme 1B. Gas evolution was noted although much less was evolved over the reaction period (8 h) than in Scheme 1A as determined by visual inspection. X-ray analysis of the product, shown in Figure 1a-ii, reveals the expected diffraction pattern of Li_2O_2. The peaks are far weaker and extensively broadened compared to those formed in the absence of carbon (Figure 1a-i). We used Ketjen black in this experiment (and in our Li-O_2 cells), which is characterized by a large surface area (1400 $m^2\ g^{-1}$) and a very high fraction of surface functional groups.[19] The greatly reduced crystallinity of the Li_2O_2 suggests that the carbon must strongly interact with the superoxide radicals generated in reaction 1 to result in physisorption on the surface, thus suppressing the dismustase reaction and nucleation of Li_2O_2. This supports recent observations that the surface chemistry of the carbon electrode substrate strongly influences the discharge products.[20]

The effect of the carbon substrate is quite different in a Li-O_2 battery (Scheme 1C), because the carbon is also the catalyst for the ORR that generates LiO_2. Figure 1a-iii shows the diffraction pattern for Li_2O_2 produced electrochemically using Ketjen black. Compared to Li_2O_2 generated using the chemical reaction described above, the "electrochemical" Li_2O_2 is much more crystalline. The coherence length is about 15−20 nm from Scherrer analysis, whereas the line broadening is so severe for the "chemical" Li_2O_2 formed in the presence of carbon that an accurate estimate of primary particle size is not possible. This contrast is also reflected in the SEM micrographs of the respective products (Figure 2). The chemically produced Li_2O_2 exhibits an amorphous, ill-defined morphology (Figure 2a and inset), in contrast to the well-defined toroids formed by electrochemically generated Li_2O_2 in the absence of catalyst (Figure 2b). Closer inspection reveals that the toroids are aggregates comprised of nanocrystalline Li_2O_2 rods with dimensions in accord with those measured from XRD analysis (see inset, Figure 2b), ~15 nm × 80 nm. These aggregate to form toroidal homogeneously sized macrostructures roughly 600−800 nm in diameter, by either epitaxial deposition or nucleated growth from the surface. The production of these

dx.doi.org/10.1021/ja2111543 | J. Am. Chem. Soc. 2012, 134, 2902−2905

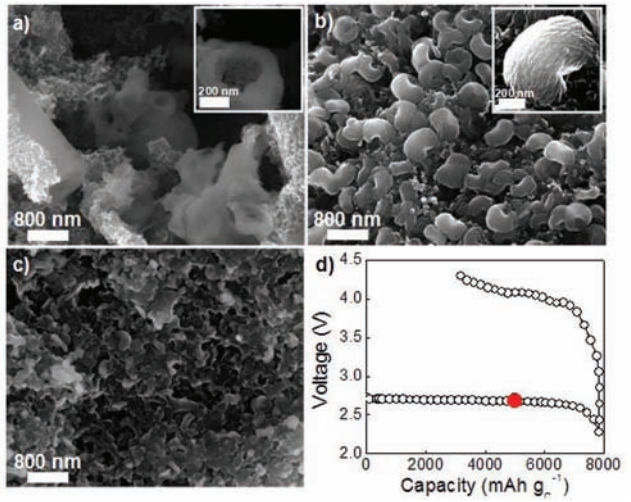

Figure 2. SEM micrographs of (a) chemical production of Li_2O_2 on carbon with $LiPF_6/KO_2$ in TEGDME; (b) electrochemical carbon/PVdF cathode discharged to 5000 mAh/g; (c) same as (b) but with α-MnO_2 catalyst, showing formation of a glassy film on the surface of the Li_2O_2; and (d) discharge/charge curve for the cathode indicating the point where the image was taken.

toroids appears only at the surface of the electrode that faces the oxygen flow; the remaining cathode area is bare.

Two factors give rise to the difference in Li_2O_2 morphology from the two routes. (1) The kinetics of precipitation favors rapid dismutation and precipitation in the chemical case due to a high LiO_2 concentration. In contrast, the electrochemical production of LiO_2 is current limited which leads to slow nucleation via an electrochemical route to form crystalline Li_2O_2. (2) The strong cathodic polarization of the carbon surface in the electrochemical cell could diminish the binding of the generated O_2^- to the substrate. This would be expected to enhance diffusion of the solvated superoxide molecules away from the surface, and favor peroxide formation by disproportionation. In either case, formation of the large toroidal aggregates on the surface suggests a short diffusion path, followed by nucleation and crystallization of Li_2O_2 very close to the sites where the superoxide is generated. A mechanism that could account for the growth of the toroids is shown in SI, Figure S6.

A prime rationale of these superoxide experiments was to explore the effect of binders and catalysts in the Li-O_2 cell. To carry this out, a solution of superoxide was first generated by the addition of KO_2/crown ether to a solution of 1 M $LiPF_6$/TEGDME, and then PVdF (a typical binder used to fabricate the porous cathode in Li-O_2 cells)[21] was added. The overall results are summarized in Scheme 1D. In sharp contrast to reaction A, gas evolution occurred for roughly 20 s, and an immediate change in the solution color to brown was observed that deepened after 1 h. The diffraction pattern of the black product that was collected (Figure 1b-i) displays the characteristic peaks of both Li_2O_2 and residual binder. To understand the dark coloration, PVdF is not stable in the presence of strong bases such as LiOH. PVdF has been reported to undergo extensive chemical dehydrofluorination with organic and alkaline bases, yielding unsaturated products with polyene structures which are responsible for the severe discoloration phenomenon.[22] The strong base abstracts the proton from the PVdF polymer backbone, followed by release of F^- to form a conjugated double bond. In our case (and by logical extension, in Li-O_2 cells), the O_2^- ion, which is a far stronger base than OH^-,[23] operates as the hydrogen abstraction agent for PVdF, and unstable HO_2 undergoes facile disproportionation to form H_2O_2, as is well established:[24]

$$LiO_{2(s)} + \text{-}(CH_2\text{-}CF_2)\text{-}_{(s)} \rightarrow HO_2 + \text{-}(CH{=}CF)\text{-}_{(s)} + LiF_{(s)} \quad (3)$$

$$2HO_2 \rightarrow H_2O_2 + O_{2(g)} \quad (4)$$

Reaction 3 is proven by the ^{13}C NMR spectrum of the brown-black product (SI, Figure S7), which reveals two new peaks we assign to the conjugated double bond at 71 (=C-H) and 170 ppm (=C-F) in addition to the residual aliphatic PVdF carbon peaks.[25] Confirmation of the production of H_2O_2 was obtained (see SI). The FT-IR spectrum also indicates the presence of the C=C double bond motif at 1522 cm^{-1} and a strong stretching peak of C=C-F at 1620 cm^{-1}, in accord with literature data for dehydrofluorinated PVdF (SI, Figure S8).[26] PVdF decomposition does not completely inhibit the production of Li_2O_2, however, implying that the superoxide radical reacts competitively with both itself and the PVdF. In a Li-O_2 cathode prepared using PVdF, access to the binder and its relative content determine the extent of reactivity. Side reactions of LiO_2 reduce the quantity of Li_2O_2 formed on discharge, and hence limit the charge capacity of the cell. On cycling of the cell, the conjugated bond motif will progressively rigidify the porous membrane structure. Furthermore, *in situ* formation of HO_2 can result in H-atom abstraction from the methylene carbons on the ether (TEGDME), which will act as a radical initiator for decomposition. This is a competitive process with the disproportionation of HO_2 to H_2O_2 (estimated to have a rate constant of 10^4 mol^{-1} s^{-1} in Me_2SO).[24]

The effect of the catalyst in the presence of LiO_2 and binder is more subtle. Some of the best catalysts for Li-O_2 ORR and OER are manganese dioxide polymorphs, including nanowire α-MnO_2. However, both LiOH and Li_2O_2 have been reported to form on discharge in the cell (in equal quantities), but the puzzle of the hydroxide remains.[16] We make similar observations in our superoxide reactions, *but only when PVdF is present* (Scheme 1E). The XRD pattern of the product from $LiPF_6$/KO_2(crown ether)/TEGDME/binder/α-MnO_2 nanowires clearly shows the reflections of both LiOH and Li_2O_2 (Figure 1b-iii). However, only Li_2O_2 is produced in the absence of either PVdF (Figure 1b-ii) or α-MnO_2 (Figure 1b-i) as discussed above. Hence we conclude both components are necessary to produce LiOH.

This phenomenon can be explained by considering the reactivity of H_2O_2 formed from decomposition of PVdF. Normally, H_2O_2 would be expected to be inert (see Scheme 1D). The diffraction pattern (Figure 1b-i) shows that the sole reaction products observed in the presence of PVdF alone are the KF and LiF salts associated with binder decomposition and Li_2O_2. Nonetheless, manganese dioxides are extremely effective H_2O_2 decomposition catalysts.[27] α-MnO_2 nanowires are expected to enable the transformation in reaction 5:

$$H_2O_2 \rightarrow H_2O_{(l)} + {}^1\!/\!_2\, O_{2(g)} \quad (5)$$

$$Li_2O_{2(s)} + 2H_2O_{(l)} \rightarrow 2LiOH_{(s)} + H_2O_2 \quad (6)$$

The water generated readily reacts with Li_2O_2 to form LiOH (reaction 6), thus accounting for its presence in the cathodes that contain both PVdF and α-MnO_2, but not either component

dx.doi.org/10.1021/ja2111543 | J. Am. Chem. Soc. 2012, 134, 2902–2905

alone (Scheme 1E). In addition, the catalyst (α-MnO_2) almost disappears from the diffraction pattern suggesting that it may decompose on reaction with H_2O_2 as claimed by Suib et al.[28]

Further proof of this account of the reactivity is found by changing the binder in the superoxide reactions. The reaction in Scheme 1E was conducted under the same conditions but using lithiated Nafion (a binder developed in recent noble-metal catalyst studies) to replace the PVdF.[29] As in Scheme 1D, no LiOH was evident in the XRD pattern (Figure 1b-iv): only Li_2O_2. Not surprisingly, the α-MnO_2 catalyst also remains.

Formation of LiOH is both significant and undesirable, as it can be a significant source of capacity fading in nonaqueous Li-O_2 cells due to the tendency to form a film on the cathode surface, blocking its catalytic activity. SEM images of porous Li-O_2 cathodes in which the products are Li_2O_2 (Figure 2c), vs those where Li_2O_2+LiOH is formed, demonstrate the "glassy" nature of the film cast on the surface. Along with concomitant production of H_2O that will react with Li_2O_2 generated in the subsequent cycle, this may deteriorate cycling of the cell. Catalyst decomposition would be detrimental to cycling.

In summary, generation of the O_2^- radical from a chemical route provides a vital probe of its reactivity with materials used in Li-O_2 cells to gauge their stability and role in determining capacity and rechargeability. Crystallization of Li_2O_2 in the absence of binder and catalyst is governed by its rate of nucleation/precipitation from LiO_2, low solubility, and interaction with the carbon surface. The electrochemical reduction of O_2 (where the rate is slow), generates nanocrystalline Li_2O_2 that aggregates to form uniformally sized ~700 nm toroids. Superoxide does not attack TEGDME significantly in the presence of O_2 but readily reacts with PVdF (or Kynar Flex), resulting in dehydrofluorination and formation of H_2O_2. In the presence of a good H_2O_2 decomposition catalyst, H_2O is produced internally in the cell which reacts with Li_2O_2 to form LiOH. In an electrochemical Li-O_2 cell, the hydroxide coats the porous cathode surface to form a film which can block further catalytic activity. Other binders such as lithiated Nafion[29] are stable with respect to O_2^- reactivity. Overall, the probe describes here serves as an easily implemented, first step route to exploring Li-O_2 battery chemistry that should be broadly applicable as a screening tool.

■ ASSOCIATED CONTENT

Supporting Information

Experimental details, NMR spectra, and suggested mechanisms. This material is available free of charge via the Internet at http://pubs.acs.org.

■ AUTHOR INFORMATION

Corresponding Author

lfnazar@uwaterloo.ca

Author Contributions

‡These authors contributed equally.

Notes

The authors declare no competing financial interest.

■ ACKNOWLEDGMENTS

This work was supported by NSERC. We thank Y. Shao-Horn (MIT), J. J. Zhang (PNNL), and S. Holdcroft (SFU) for helpful discussions.

■ REFERENCES

(1) Abraham, K. M.; Jiang, Z. *J. Electrochem. Soc.* **1996**, *143*, 1.
(2) Ogasawara, T.; Debart, A.; Holzapfel, M.; Novak, P.; Bruce, P. G. *J. Am. Chem. Soc.* **2006**, 1390.
(3) Debart, A.; Paterson, J.; Bao, J.; Bruce, P. G. *Angew. Chem.* **2008**, 4521.
(4) Debart, A.; Bao, J.; Armstrong, R.; Bruce, P. G. *J. Power Sources* **2007**, 1177.
(5) Lee, J. S.; Kim, S. T.; Cao, R.; Choi, N. S.; Liu, M.; Lee, K. T.; Cho, J. *Adv. Energy Mater.* **2011**, *1*, 34. Kraytsberg, A.; Ein-Ali, Y. *J. Power Sources* **2011**, *196*, 886.
(6) Read, J. *J. Electrochem. Soc.* **2002**, A1190.
(7) Laoire, C. O.; Mukerjee, S.; Abraham, K. M. *J. Phys. Chem. C* **2009**, *113*, 20127.
(8) Laoire, C. O.; Mukerjee, S.; Plichta, E. J.; Hendrickson, M. A.; Abraham, K. M. *J. Electrochem. Soc.* **2011**, A302.
(9) Mizuno, F.; Nakanishi, S.; Kotani, Y.; Yokoishi, S.; Iba, H. *Electrochemistry* **2010**, *78*, 403.
(10) Lu, Y.-C.; Kwabi, D. G.; Yao, K. P. C.; Harding, J. R.; Zhou, J.; Zuin, L.; Shao-Horn, Y. *Energy Environ. Sci* **2011**, *4*, 2999.
(11) McCloskey, B. D.; Bethune, D. S.; Shelby, R. M.; Girishkumar, G.; Luntz, A. C. *J. Phys. Chem. Lett.* **2011**, *2*, 1161.
(12) Xu, W.; Viswanathan, V. V.; Wang, D. Y.; Towne, S. A.; Xiao, J.; Nie, Z. M.; Hu, D. H.; Zhang, J. G. *J. Power Sources* **2011**, *196*, 3894.
(13) Veith, G. M.; Dudney, N. J.; Howe, J.; Nanda, J. *J. Phys. Chem. C* **2011**, *115*, 14325.
(14) Freunberger, S.; Chen, Y.; Peng, Z.; Griffin, H.; Hardwick, L.; Bardé, F.; Novak, P.; Bruce, P. G. *J. Am. Chem. Soc.* **2011**, *133*, 8040.
(15) Oh, S. H.; Yim, T.; Pomerantseva, E.; Nazar, L. F. *Electrochem. Solid State Lett.* **2011**, *14*, A185.
(16) Freunberger, S.; Chen, Y.; Drewett, N.; Hardwick, L.; Bardé, F.; Bruce, P. G. *Angew. Chem., Int. Ed.* **2011**, *50*, 1.
(17) Assary, R. S.; Curtiss, L. A.; Redfern, P. C.; Zhang, Z. C. *J. Phys. Chem. C* **2011**, *115*, 12216.
(18) Filippo, J.; Chern, C.; Valentine, J. *J. Org. Chem.* **1975**, 1680.
(19) Arico, A. S.; Antonucci, V.; Minutoli, M.; Giordano, N. *Carbon* **1989**, *27*, 337.
(20) Peng, Z.; Freunberger, S.; Hardwick, L.; Chen, Y.; Giordani, V.; Barde, F.; Novak, P.; Graham, D.; Tarascon, J. M.; Bruce, P. G. *Angew. Chem., Int. Ed.* **2011**, 6351.
(21) Albertus, P.; Girishkumar, G.; McCloskey, B.; Sanchez-Carrera, R.; Kozinsky, B.; Christensen, J.; Luntz, A. C. *J. Electrochem. Soc.* **2011**, A343. Li, Y.; Wang, J.; Li, X.; Geng, D.; Li, R.; Sun, X. *Chem. Commun.* **2011**, *47*, 9438. Hassoun, J.; Croce, F.; Armand, M.; Scrosati, B. *Angew Chem., Int. Ed.* **2011**, 1. Beattie, S.; Manolescu, S.; Blair, S. *J. Electrochem. Soc.* **2009**, A44.
(22) Brynaert, J.; Jongen, N.; Dewez, J. L. *J. Polym. Sci. A* **1996**, 1227. Maccone, P.; Brinati, G.; Arcella, V. *Polym. Eng. Sci.* **2000**, 761.
(23) Sawyer, D.; Valentine, J. *Acc. Chem. Res.* **1981**, 393.
(24) Sawyer, D; Roberts, J. L.; Calderwood, T. S.; Sugimoto, H.; McDowell, M. S. *Philos. Trans. R Soc. London B: Biol. Sci.* **1985**, *311*, 483.
(25) Danks, T. N.; Slade, R. C. T.; Varcoe, J. R. *J. Mater. Chem.* **2003**, *13*, 712.
(26) Zulfiqar, S.; Zulfiqar, M.; Rizvi, M.; Munir, A. *Polym. Degrad. Stab.* **1994**, *43*, 423.
(27) Broughton, D.; Wentworth, R. *J. Am. Chem. Soc.* **1947**, 741.
(28) Benbow, E. M.; Kelly, S. P.; Zhao, L.; Reutenauer, J. W.; Suib, S. L. *J. Phys. Chem.* **2011**, *115*, 22009.
(29) Lu, Y.-C.; Xu, Z.; Gasteiger, H. A.; Chen, S.; Hamad-Schifferli, K.; Shao-Horn, Y. *J. Amer. Chem. Soc.* **2010**, *132*, 12170.